



HAL
open science

An ALE three-dimensional model of orthogonal and oblique metal cutting processes

Olivier Pantalé, Roger Rakotomalala, Maurice Touratier

► **To cite this version:**

Olivier Pantalé, Roger Rakotomalala, Maurice Touratier. An ALE three-dimensional model of orthogonal and oblique metal cutting processes. *International Journal of Forming Processes*, 1998, 1 (3), pp.371-388. hal-03485267

HAL Id: hal-03485267

<https://hal.science/hal-03485267>

Submitted on 17 Dec 2021

HAL is a multi-disciplinary open access archive for the deposit and dissemination of scientific research documents, whether they are published or not. The documents may come from teaching and research institutions in France or abroad, or from public or private research centers.

L'archive ouverte pluridisciplinaire **HAL**, est destinée au dépôt et à la diffusion de documents scientifiques de niveau recherche, publiés ou non, émanant des établissements d'enseignement et de recherche français ou étrangers, des laboratoires publics ou privés.



Open Archive Toulouse Archive Ouverte (OATAO)

OATAO is an open access repository that collects the work of Toulouse researchers and makes it freely available over the web where possible.

This is an author-deposited version published in: <http://oatao.univ-toulouse.fr/>
Eprints ID: 5390

To cite this version:

Pantalé, Olivier and Rakotomalala, Roger and Touratier, Maurice *An ALE three-dimensional model of orthogonal, oblique metal cutting processes*. (1998) International Journal of Forming Processes, vol.1 (n° 3). pp. 371-388. ISSN 1292-7775

Any correspondence concerning this service should be sent to the repository administrator: staff-oatao@listes.diff.inp-toulouse.fr

AN ALE THREE-DIMENSIONAL MODEL OF ORTHOGONAL AND OBLIQUE METAL CUTTING PROCESSES

Olivier Pantalé⁺, Roger Rakotomalala⁺, Maurice Touratier*

⁺ L.G.P C.M.A.O - E.N.I.T, 47 Av d'Azereix BP 1629 - 65016 Tarbes cedex

* LM²S UA CNRS 1776, ENSAM, 151 bd de l'hôpital 75013 Paris

An Arbitrary Lagrangian Eulerian (ALE) approach is used in this paper to model continuous three-dimensional orthogonal and oblique steady-state metal cutting processes. The thermo-mechanical coupled model includes the effects of elastoplasticity, high strain and strain rates, heat generation and friction between the chip and the tool. A thermal-viscoplastic constitutive equation associated with the Johnson-Cook flow law is adopted for the workpiece. A classic Coulomb friction law associated with heat generation and heat transfer is used to model the tool-chip contact. The model is suitable for predicting thermo-mechanical quantities, chip geometry and the cutting forces from a set of cutting data, material and contact parameters. Cutting experiments and numerical simulations were performed on a 42CD4 steel and comparisons show a reasonable level of agreement.

KEYWORDS: machining, finite elements, finite volumes, ALE, thermo-mechanical coupling

1. Introduction

Experimental observations of metal cutting processes show that the phenomena associated with chip formation are full of complexities. The cutting material is subjected to high strains, high strain rates and high temperatures while the cutting tool is subjected to wear as a consequence of very localized high pressures and high temperature gradients. The influence of cutting temperature distribution on tool wear is a well known fact since Taylor's works. Tay [TAY 93] shows that the craterization of the tool flank face is directly related to the temperature distribution. Even though a lot of experimental research about tool flank face temperature measurements has been done in recent years [LEZ 90], the issue is still full of complexities. Yet the issue is full of complexities. The aim of our study is therefore to develop a predictive numerical model suitable for obtaining stresses and temperature distributions in the tool-chip contact zone, from the set of cutting and material parameters.

Many research projects about numerical simulation of cutting processes have been done in the last few years, and a number of models are presented in the literature. Over the last five years, friction and wear effects have been included in numerical models like the one presented by Komvopoulos et al. [KOM 91] where the authors study the influence of the coefficient of friction and the craterization of the tool flank face on the resulting geometry and cutting forces. Another interesting model is the one presented by Younis et al. [YOU 92] where the authors' interest is to develop a numerical model suitable for predicting thermal and mechanical stresses in the tool from a thermal and mechanical set of data as boundary conditions. Tay et al. [TAY 91] have developed a purely thermal model, from a set of experimental results, to predict mechanical variations of the tool characteristics. Ueda et al. [UED 93] present a three-dimensional model (suitable for predicting the chip geometry and the cutting forces) based on a rigid-plastic finite element method. Oblique cutting process simulations are presented in this paper.

Rakotomalala et al. [RAK 93] present a predictive ALE two-dimensional model suitable for predicting geometry and cutting forces from a set of material and cutting parameters. The model presented in our paper is based on the same approach and constitutes the next step of this study.

One of the earlier models is that presented by Marushich et al. [MAR 95] where the authors present a numerical two-dimensional model of an orthogonal metal cutting process including crack propagation, suitable for modelling non continuous chip formation.

In this paper, we present a three-dimensional numerical model of orthogonal and of oblique metal cutting processes. Both are based on an Arbitrary Lagrangian Eulerian (ALE) approach, generally dedicated to fluid simulations. The ALE formulation has been used by several authors [HUE 90] in metal forming simulations in order to overcome problems encountered while using a purely Lagrangian or Eulerian method. But this model is one of the first application of such an approach to cutting simulation. Briefly speaking, the use of this approach combines the advantages of both classic representations in a single description which can be considered as an automatic and continuous rezoning method.

In this paper we first present a brief review of the ALE governing equations and the associated forms of the conservation laws. We will then present the constitutive law and the contact algorithm used in the model followed by spatial and time discretization. Two applications will then be presented. The first concerns a three-dimensional model of orthogonal metal cutting process, whereas the second deals with an oblique model simulation. Comparisons with experimental results are also given in this part.

2. ALE formulation

An Arbitrary Lagrangian Eulerian formulation is an extension of both classic Lagrangian and Eulerian ones where grid points may have an arbitrary motion. In such

a description, material points are represented by a set of Lagrangian coordinates \vec{X} , spatial points with a set of Eulerian coordinates \vec{x} , and reference points (grid nodes) with a set of Arbitrary coordinates $\vec{\xi}$. We illustrate this graphically in Figure 1. At time t , \vec{x} is simultaneously the image of \vec{X} by the material motion $\vec{x} = \Psi(\vec{X}, t)$, and $\vec{\xi}$ by the grid motion $\vec{x} = \hat{\Psi}(\vec{\xi}, t)$.

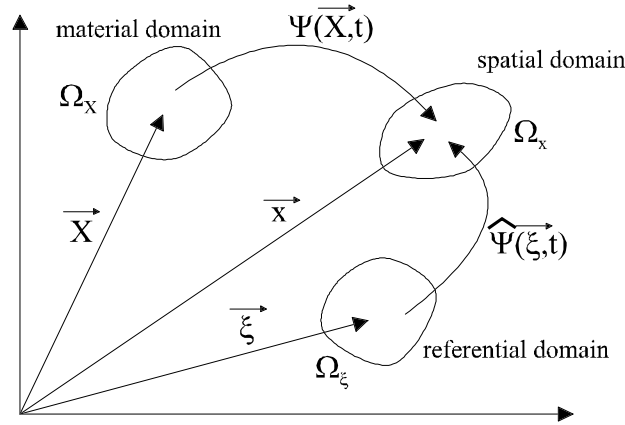


Figure 1. Motion description in ALE

All physical quantities are computed at geometrical points \vec{x} at time t . All conservation laws must be expressed taking into account the meshing evolution during the calculation. Considering a space and time dependent quantity f , one must express all the conservation laws using the material (\dot{f}), spatial (f') and mixed ($\overset{\circ}{f}$) derivatives of a quantity f defined below:

$$\dot{f} = \frac{\partial f}{\partial t} \Big|_{\vec{X}=cte}, \quad f' = \frac{\partial f}{\partial t} \Big|_{\vec{x}=cte}, \quad \overset{\circ}{f} = \frac{\partial f}{\partial t} \Big|_{\vec{\xi}=cte} \quad [1]$$

Conservation laws are usually written using material derivatives in an Eulerian formulation. Therefore, Hughes [HUG 81] introduced the relationship below between material and mixed derivatives as:

$$\dot{f} = \overset{\circ}{f} + f_{,i} c_i \quad [2]$$

where $c_i = v_i - \hat{v}_i$ is a convective term representing the relative velocity between the material (v_i) and mesh (\hat{v}_i) velocities and $f_{,i}$ represents the derivative of f with respect to direction i .

It is easy to establish the following relationship between material (\dot{K}) and mixed ($\overset{\circ}{K}$) derivatives of a volume integral of a function f as:

$$\dot{K}(t) = \overset{\circ}{K}(t) + \int_{\omega_t} (f c_i)_{,i} d\omega_t \quad [3]$$

Therefore, ALE integral forms of the conservation laws are directly obtained from classical Eulerian ones using [3], and local ALE forms with [2] as shown below, for example in Cartesian coordinates (initial and boundary conditions have of course to be added):

$$\overset{\circ}{\rho} + \rho v_{i,i} + \rho_{,i} c_i = 0 \quad (mass) \quad [4]$$

$$\rho \overset{\circ}{v}_i + \rho v_{i,j} c_j = f_i + \sigma_{ij,j} \quad (momentum) \quad [5]$$

$$\rho \overset{\circ}{e} + \rho e_{,i} c_i = r - q_{i,i} + \sigma_{ij} v_{i,j} \quad (energy) \quad [6]$$

In these equations, ρ is the mass density, \vec{q} the heat flux, \vec{f} the body force vector (taken equal to zero hereafter), σ the Cauchy stress tensor, r the body heat generation (taken equal to zero hereafter) and e the specific internal energy.

3. Constitutive and contact laws

A thermo-elastoplastic constitutive equation associated with the Johnson-Cook flow law is adopted for the workpiece while a Coulomb friction law including heat generation and heat transfer is used for the tool-chip contact.

3.1. Constitutive equation

A constitutive equation used in cutting models must take into account plasticity or visco-plasticity, temperature, strain rate and damage, if we want to simulate discontinuous chip formation. In this paper, the numerical model adopted is suitable for simulating continuous steady-state metal cutting processes as a thermo-elastoplastic constitutive equation associated with the Johnson Cook flow law has been adopted. In large strain formulations, the well known strain rate decomposition isn't allowed. One must introduce an intermediate configuration obtained by stress relaxation, and the partition of the strain rate gradient tensor \mathbb{L} is then given by Lee et al. [LEE 80] as:

$$\mathbb{L} = \mathbb{L}^e + \mathbb{V}^e \mathbb{L}^p (\mathbb{V}^e)^{-1} \quad [7]$$

where \mathbb{V}^e is the pure strain tensor associated with the relaxed configuration (i.e. $\mathbb{F}^e = \mathbb{V}^e \mathbb{R}^e$). When an elastic deformation is small, Equation [7] can be written as $\mathbb{L} \simeq \mathbb{L}^e + \mathbb{L}^p$, leading to the strain rate tensor \mathbb{D} decomposition below:

$$\mathbb{D} = \mathbb{D}^e + \mathbb{D}^p \quad \text{with} \quad \begin{cases} \mathbb{D}^e = \text{sym}(\mathbb{L}^e) \\ \mathbb{D}^p = \text{sym}(\mathbb{L}^p) \end{cases} \quad [8]$$

In order to satisfy objectivity, the constitutive law is written using the Jaumann

derivative of the Kirchhoff stress tensor $\overset{\circ}{\mathbb{T}}$ and the strain rate tensor \mathbb{D} . When elastic strains are small ($\mathbb{T} \simeq \boldsymbol{\sigma}$) constitutive equations can be expressed using \mathbb{D} and $\overset{\circ}{\boldsymbol{\sigma}}$. Therefore, in large strain formulations, the following constitutive equation is given by the set of relationships:

$$\overset{\circ}{\mathbb{S}} = \mathbb{C} : \mathbb{D}; \quad \overset{\circ}{\boldsymbol{\sigma}} = \dot{P} \mathbb{I} + \overset{\circ}{\mathbb{S}} \quad [9]$$

where \mathbb{S} is the deviatoric part of the stress tensor $\boldsymbol{\sigma}$, P the hydrostatic pressure, \mathbb{I} the second order identity tensor and \mathbb{C} the constitutive tensor defined by:

$$\begin{cases} \mathbb{C} = \mathbb{C}^e = 2\mu \left(\mathbb{J} - \frac{1}{3} \mathbb{I} \otimes \mathbb{I} \right) & \text{if } f = 0 \text{ and } \dot{f} < 0, \text{ or } f < 0 \\ \mathbb{C} = \mathbb{C}^{ep} = 2\mu \left(\mathbb{J} - \frac{1}{3} \mathbb{I} \otimes \mathbb{I} - \gamma (\mathbb{N} \otimes \mathbb{N}) \right) & \text{if } f = 0 \text{ and } \dot{f} \geq 0 \end{cases} \quad [10]$$

where \mathbb{J} is the fourth order identity tensor, μ the Lamé coefficient, γ the tangential hardening coefficient, $\mathbb{N} = \frac{\bar{\boldsymbol{\sigma}} \otimes \bar{\boldsymbol{\sigma}}}{\sqrt{\bar{\boldsymbol{\sigma}} : \bar{\boldsymbol{\sigma}}}}$ and $f = \bar{\boldsymbol{\sigma}} - R$ the flow law with $\bar{\boldsymbol{\sigma}}$ the Von-Mises equivalent stress and R given by the Johnson-Cook criterion [JOH 83]:

$$R = (A + B \bar{\boldsymbol{\varepsilon}}^n) \left(1 + C \ln \frac{\dot{\bar{\boldsymbol{\varepsilon}}}}{\dot{\bar{\boldsymbol{\varepsilon}}}_0} \right) \left(1 - \left(\frac{T - T_0}{T_{melt} - T_0} \right)^m \right) \quad [11]$$

where $\bar{\boldsymbol{\varepsilon}}$ is the equivalent strain, $\dot{\bar{\boldsymbol{\varepsilon}}}$ the equivalent strain rate, T the temperature and $A, B, C, T_0, T_{melt}, n, m, \dot{\bar{\boldsymbol{\varepsilon}}}_0$ are material coefficients given in Table 1.

Using the fundamental relation [2] linking material and mixed derivatives, we may obtain the ALE form of the constitutive equation below:

$$\begin{cases} \overset{\circ}{\mathbb{S}} = \mathbb{C} : \mathbb{D} - \vec{c} \cdot \nabla \mathbb{S} + \mathbb{W} \mathbb{S} - \mathbb{S} \mathbb{W} \\ \dot{P} = \dot{P} - \vec{c} \cdot \nabla P \end{cases} \quad [12]$$

where \mathbb{W} is the spin tensor and ∇ the gradient operator symbol. On the one hand, relationships [12] insure the objectivity of the constitutive equation, and on the other hand they allow the stress tensor transport (by the term $\vec{c} \cdot \nabla \mathbb{S}$) resulting from the motion between material and grid points.

3.2. Contact law

In a metal cutting process, because of high stresses, high strain rates and high temperatures, a high mechanical power is dissipated in the tool-chip interface thus leading to many structural modifications of the contacting pieces. Therefore, Shih [SHI 93] shows that no universal contact law exists which can predict friction forces among a wide range of cutting conditions. Experience actually shows that stick and slip zones along the interfacial zone between the chip and the tool depend on cutting conditions, pressure, temperature, etc [CHI 90].

In our model, a classic Coulomb friction law is assumed to model the tool-chip and the tool-workpiece contact zone. The stick/slip conditions are given by:

$$\begin{array}{ll} \text{stick} & |T_t| < C_f |T_n| \\ \text{slip} & |T_t| = C_f |T_n| \end{array}$$

where T_n and T_t represent respectively the normal and tangential components of the surface traction at the interface and C_f is the coefficient of friction assumed as a constant depending on the nature of the contacting bodies.

The explicit integration algorithm used in our model allows taking the contact between the two bodies into account by adding an external force vector to the contacting nodes. This can be done by the introduction of an \mathbb{F}^{ext} vector in the right member of the momentum conservation law. Normal components of this force vector are set equal so as to prevent penetration and the tangential component is set with respect of the Coulomb friction law defined above.

The contact algorithm also includes thermal capacities. Heat generation and heat transfer at the interface are taken into account. The heat generation in the slipping contact surface is given by:

$$dQ_{fric} = |T_t| |V_t| dt$$

where V_t is the tangential slip velocity (i.e. relative velocity between the two contacting bodies). According to the explicit scheme, calculated heat flux is then reintroduced as an external thermal flux for each contacting node.

Generated heat flux is divided among pieces in contact in a ratio depending on the thermal features of both pieces, geometry and sliding conditions. Therefore, to model thermal behavior, one may introduce a thermal resistance R_{th} (to model the thermal discontinuity at the interface) and a sharing coefficient α (to model the ratio), but the experimental identification of such a coefficient is full of complexities. Experimental studies [BAR 94] about thermal resistance show that the affected value may vary within a wide range with contact conditions and slipping speed V_t . In the simplest case, when solids are in perfect contact, the Vernotte relation may be used to determine the α coefficient as a function of material effusivities. Numerical simulations about the relative importance of α and R_{th} have been done and show that a variation of R_{th} has no significant effect on the result, and on the contrary, the model is quite sensitive to the α coefficient. In our model we assumed a thermal resistance and a sharing coefficient of 0.0 and 0.5 respectively.

4. Discretization

A finite element method (FEM) is adopted for the discretization of the momentum equation, while a finite volume method (FVM) is used for the discretization of the mass and the energy equations because of simplicity. An explicit integration scheme is adopted for time discretization.

4.1. Momentum equation

The associated weak form of the momentum equation is deduced by pre-multiplying the equation [5] by a weighting function v_i^* over the spatial domain $\Omega(t)$ with the boundary $\Gamma(t)$. We then use the divergence theorem so as to include surface forces and a classic Galerkin approach to discretize the equation. The presence of convective terms in the ALE form of the momentum equation leads to numerical difficulties linked to the non symmetric character of the convective operators. Therefore, the use of a non centered integration scheme (upwind technique) for the discretization of the convective term is adopted in the model instead of the introduction of a numerical dissipation. Also, when using an explicit integration scheme, the cost of the calculation is directly linked to the efficiency of the numerical integration scheme. One of the most efficient methods is to use a single point integration element associated with a stability algorithm to prevent hourglass modes. The policy in our model is to add an hourglass resisting force vector, as Koslov [KOS 78] in the momentum equation.

After taking into account these remarks, the corresponding matrix form of the momentum equation is given by:

$$\mathbb{M}^* \cdot \overset{\circ}{\mathbf{v}} = \mathbb{F}^{ext} - \mathbb{F}^{int} - \mathbb{F}^c + \mathbb{F}^{hgr} \quad [13]$$

where \mathbf{v} is the material speed, \mathbb{F}^{ext} is the external force vector, \mathbb{F}^{int} is the internal force vector (including the contact forces), \mathbb{F}^c is the convective vector, \mathbb{F}^{hgr} is the hourglass resisting force vector and \mathbb{M}^* is the lumped form of the mass matrix. Convective vector force \mathbb{F}^c is defined as a weighted function of the convective tensor \mathbb{K}^c by an upwind coefficient matrix γ_{ij}^e .

$$\mathbb{F}_i^c = \sum_e \gamma_{ij}^e \cdot \mathbb{K}_{ij}^{ce} \mathbf{v}_j \quad \text{with} \quad \begin{cases} \mathbb{K}_{ij}^{ce} = \int_{\Omega_e^h} (\rho \mathbb{N}_{\alpha i} \mathbb{N}_{\alpha j, \beta} c_\beta) d\Omega_e^h \\ \gamma_{ij}^e = 1 + \eta \operatorname{sgn} \left(\int_{\Omega_e^h} (\mathbb{N}_{ij, \beta} c_\beta) d\Omega_e^h \right) \end{cases} \quad [14]$$

where \mathbb{N} is defined by the shape functions, $\eta \in [0, 1]$ represents the upwind coefficient ($\eta = 0$ defines a centered integration scheme, $\eta = 1$ defines a full-upwind one). Weighting functions γ_{ij}^e defined in Equation [14] include relative motion between material and grid points from the introduction of the convective term \overrightarrow{c} .

4.2. Mass and energy equations

Mass and energy equations are both discretized using a finite volume method (FVM). The domain is discretized into a set of cells (see Figure 2) and quantities are assumed as constant over the volume integrals. A total compatibility between FVM and FEM is ensured by setting identical control volumes and finite elements.

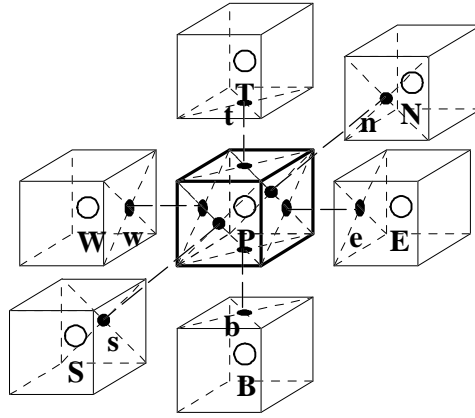


Figure 2. A finite volume cell and 6 neighbours

Discretized forms of conservation laws are obtained directly from Equations [4] and [6] by using a finite volume formulation:

$$\overset{\circ}{\rho}_P V + \sum_{\alpha=n,s,e,w,t,b} A_\alpha \rho_\alpha \vec{c} \cdot \vec{n}_\alpha = 0 \quad [15]$$

$$(\overset{\circ}{\rho}_P e_P) V = V (\sigma_{ij} D_{ij})_P + \sum_{\alpha=n,s,e,w,t,b} A_\alpha (\vec{q} - \rho_\alpha e_\alpha \vec{c}) \cdot \vec{n}_\alpha \quad [16]$$

where V is the volume of the cell, A_α is the surface of the lateral face α , n_α is the external normal of the lateral face α , ρ_P and e_P are values of ρ and e computed at point P (pole of the cell). ρ_α and e_α are the values of ρ and e calculated at the center of each face of the cell. In order to treat convective terms, one may use an upwind technique to evaluate these quantities. As an example and according to the notation of Figure 2, the calculation of the ρ_e value corresponding to the *east* face is given by the relationship below:

$$\rho_e = \frac{1}{2} [\rho_P (1 - \eta \cdot \text{sgn}(\vec{c} \cdot \vec{n}_e)) + \rho_E (1 + \eta \cdot \text{sgn}(\vec{c} \cdot \vec{n}_e))] \quad [17]$$

where $\eta \in [0, 1]$ is an upwind coefficient. $\eta = 0$ gives a centered integration scheme while $\eta = 1$ corresponds to a full upwind scheme.

For the energy equation, Fourier's law is adopted for the conduction term and the specific internal energy e is linked to the temperature T using the relationship $de = C_p \cdot dT$, where C_p is the specific heat coefficient.

4.3. Time integration

Concerning time integration, a third order explicit central difference scheme is used. The time increment Δt is subjected to the Courant stability criteria defined by $\Delta t \leq \Delta t_{crit}$ where Δt_{crit} is a function of the sound and convective speeds.

Arbitrary Lagrangian Eulerian formulation also requires the use of an appropriate grid motion control algorithm. Grid speed at node I at the end of an increment is given by the Giuliani [DON 82] relationship below:

$$\hat{v}_I^{t+\frac{\Delta t}{2}} = \frac{1}{N} \sum_{J=1}^N \hat{v}_J^{t-\frac{\Delta t}{2}} + \frac{1}{N^2} \frac{\alpha}{\Delta t} \sum_{J=1}^N L_{IJ}^t \sum_{K=1}^N \frac{\hat{u}_I^t - \hat{u}_K^t}{L_{IK}} \quad [18]$$

where N is the number of nodes connected to node I , L_{IJ} is the distance between nodes I and J , \hat{u} is the grid displacement, and α is an upwind coefficient. Knowledge of the grid speed \hat{v} allows us to compute the convective speed \vec{c} used in ALE formulations and the four unknown vectors \mathbb{F}^c , \mathbb{F}^{int} , \mathbb{F}^{ext} , \mathbb{F}^{hgr} at any given time t . Then, integrating successively the three conservation laws (momentum, mass and energy) gives the unknown values of $\vec{v}(t + \Delta t)$, $\rho(t + \Delta t)$, and $e(t + \Delta t)$ respectively. Finally, integrating the constitutive law given by [12] allows us to determine stress tensor $\sigma_{ij}(t + \Delta t)$ using explicit elastic predictions and a radial return algorithm.

5. Numerical simulations

Two numerical simulations are presented in this paper to illustrate steady state orthogonal and oblique metal cutting of a 42CD-4 steel with a tungsten carbide tool (SECO TPGN-160302 P10 tool). The use of a three-dimensional approach allows taking into account boundary effects in the transverse direction.

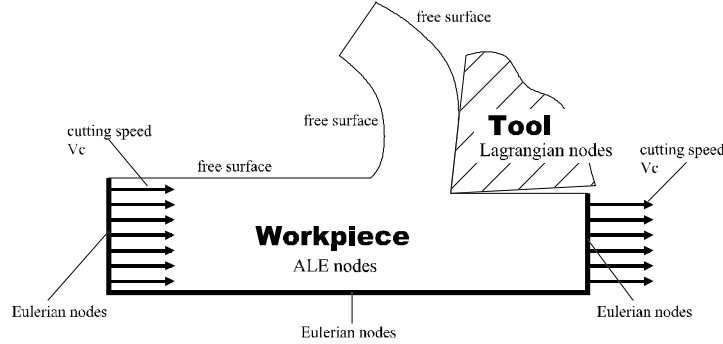


Figure 3. Boundary conditions of the finite element model

Neither geometry of the chip nor the contact length are known at the beginning of the calculation. In our model we introduced an arbitrary initial geometry deduced from a two-dimensional simulation which is updated during the computation with a view to reduce simulation time. Here, the workpiece is modeled using an ALE formulation while the tool is rigid and Lagrangian (see Figure 3 for details). We used a Master/Slave algorithm for the tool-chip contact.

In addition to the ALE nodes of the workpiece, a typical finite element mesh contains purely Eulerian or purely Lagrangian nodes. By definition, an Eulerian node has a zero grid velocity ($\hat{v} = 0$) while a Lagrangian node moves with the corresponding material node ($\hat{v} = v$). The description of the free-surfaces of the model uses nodes which are simultaneously Lagrangian in the normal direction and Eulerian in the tangential direction allowing a continuous update of the free surface location until the steady-state condition is reached. This means that the normal component of the material velocity reaches zero. In this sense, the model is equivalent to an Eulerian one when the steady state solution is obtained (see [JOY 98] for further details).

Concerning the thermal boundary condition, we assumed that all surfaces are adiabatic except for the contact surface where the heat flux created by the friction is prescribed. In the discretized Equation [16], the calculated heat flux is included in the term \vec{q} .

5.1. Orthogonal model

The first application concerns a three-dimensional steady-state simulation of the orthogonal metal cutting process as illustrated in Figure 4a. The material properties of the tool and workpiece are reported in Table 1, and the process characteristics are given in Table 2.

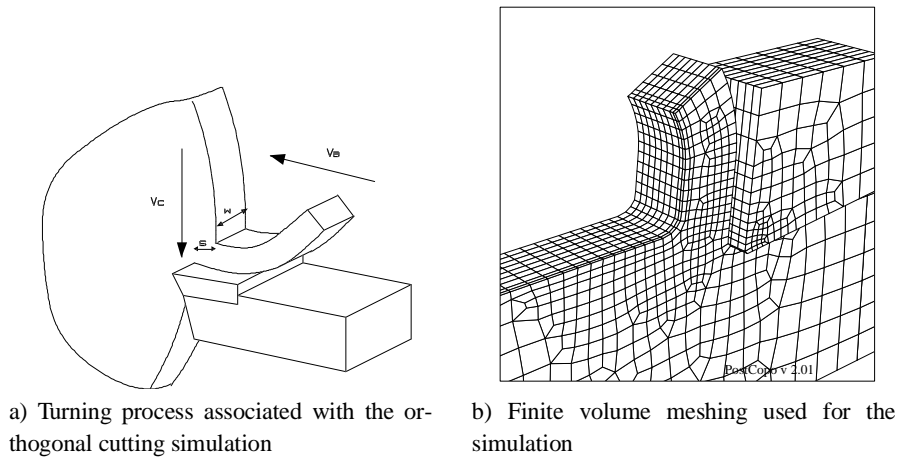


Figure 4. *Turning process and associated model meshing*

A	595 <i>Mpa</i>		
B	580 <i>Mpa</i>		
C	0.023	%WC	56 %
T_0	300°K	%TiC	20 %
T_{melt}	1793°K	%TaC	14 %
m	13	%Co	9 %
n	0.133	Young modulus E	630 <i>GPa</i>
$\frac{\bullet}{\varepsilon_0}$	10 ³	Shear modulus G	1600 <i>Mpa</i>
mass density ρ	7850 <i>kg/m³</i>	mass density ρ	14950 <i>kg/m³</i>
specific heat C_p	358 <i>J/kg°K</i>	specific heat C_p	198 <i>J/kg°K</i>
conductivity λ	38 <i>W/m°K</i>	conductivity λ	100 <i>W/m°K</i>
<i>Workpiece parameters (42CD4 steel)</i>		<i>Tool parameters</i>	

Table 1. Material parameters

cutting speed V_c	4.0 <i>m/s</i>	rake angle	5°
advancing speed V_a	0.50 <i>mm/rev</i>	flank angle	6°
depth of cut	2.0 <i>mm</i>	bevelled edge	0.07 <i>mm</i>
<i>Machining conditions</i>		<i>Tool geometry</i>	

Table 2. Cutting parameters

The friction coefficient $C_f = 0.32$ has been obtained from an experimental apparatus by applying a normal force on a tool in contact with the rotating workpiece, and measuring the corresponding tangential forces [JOY 98]. The thermal properties of the tool are supposed to be matched to those of the workpiece, giving an equal proportion of frictional heat allotted to the tool and the chip according to the Vèrnotte relationship linking the sharing coefficient α and the material effusivities of the two contacting bodies.

The ALE explicit approach presented above has been adopted to solve the metal-cutting problem. Figure 4b shows the meshing used for the numerical simulation where only half of the structure is modelized because of the symmetry plane. The meshing used here is about 6400 nodes and 5200 elements. Concerning the convergence, the accuracy of the finite element technique depends on the size of the mesh; a model with more refined mesh in the contact and tip tool zones does not change the results appreciably (3% of variation for the maximum temperature between "5200 elements" and "5550 elements" models). Time steps are of the order of $5 \cdot 10^{-9}s$ which necessitates $8 \cdot 10^5$ steps (i.e. a total CPU time between 3 and 4 days on a Silicon Graphics R4000 Indigo). Numerical results are reported in Table 3. Contact length L_{cont} , chip inner radius R_{int} and lateral dilatation of the chip have been measured straight on the meshing using home-made post-processor facilities.

Figure 6 shows the lateral expansion of the material in the direction orthogonal to the cutting plane (i.e. the plane formed by cutting and advancing speeds V_c and V_a). Figure 5 shows the time-history temperature plot of some selected nodes on the

tool flank face. From the latter, we can see that all temperatures have reached their stationary values (an average of $800^{\circ}C$) after 2 milliseconds of simulated machining time. Figure 7a presents the temperature contour plot on the tool flank face. Well known experimental results show that maximum temperature is not located along the edge but on the flank face of the tool, at a distance $L_{T_{max}}$ from the edge (more or less equal to the advancing "depth of cut" value). Comparisons (reported in Table 3) of experimental measurements of the cutting and advancing forces with numerical ones show a very good agreement. Table 3 also reports calculated temperatures in the secondary shear zone and comparison with an analytical result obtained using the Oxley model. The Oxley model gives directly the average temperature in the secondary shear zone, therefore an average temperature computation in the corresponding area has been done in the numerical model for comparison reasons.

Experimental three-dimensional mappings of the tool flank face (see Figure 7b) have also been done and measurements are reported in Table 4. Measured distance d_{crater} represents the distance between the center of the crater on the tool flank face and the edge of the tool, while $L_{T_{max}}$ is the distance between the center of the element, where T_{max} is reached, and the edge of the tool. Comparisons of experimental value of d_{crater} and calculated $L_{T_{max}}$ distance (reported in Table 3) therefore show a very good level of agreement. Comparing Figures 7a and 7b illustrates the existing correlation given by Tay [TAY 93] between temperature and wear on the tool flank face.

F_c	2.209 kN	$T_{tool_{max}}$	$740^{\circ}C$	F_c	2.150 kN
F_a	0.690 kN	$T_{chip_{max}}$	$910^{\circ}C$	F_a	0.720 kN
L_{cont}	1.00 mm	$L_{T_{max}}$	533 μm	d_{crater}	530 μm
R_{int}	2.25 mm	dilatation	14%	$T_{chip_{Oxley}}$	$936^{\circ}C$
<i>Numerical results</i>				<i>Experimental results</i>	

Table 3. Comparison of numerical results and experimental measurements

analysed surface	2.412 x 4.020 μm
depth of crater	41 μm
width of crater	620 μm
measured d_{crater}	530 μm

Table 4. Experimental measurements from the 3D mapping of the tool flank face

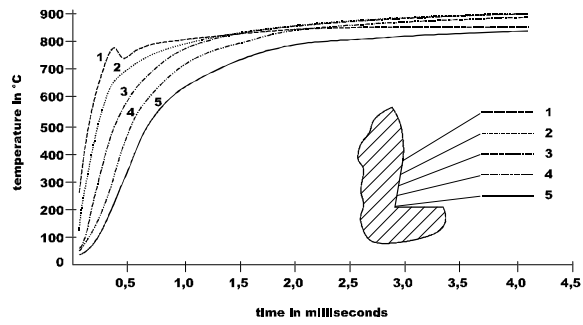


Figure 5. Time-history of the temperatures along the tool-chip contact zone for 5 selected points

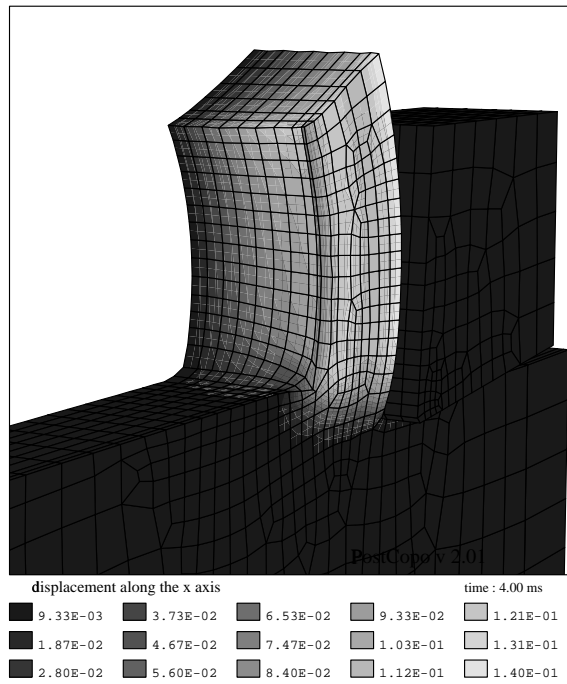
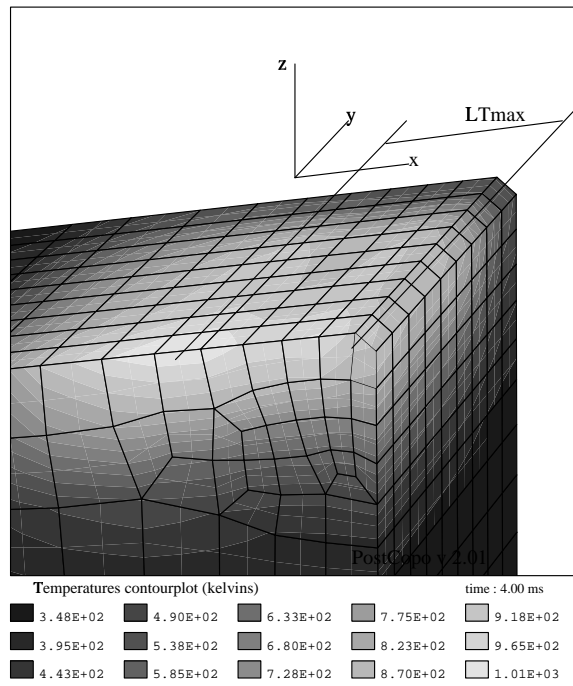
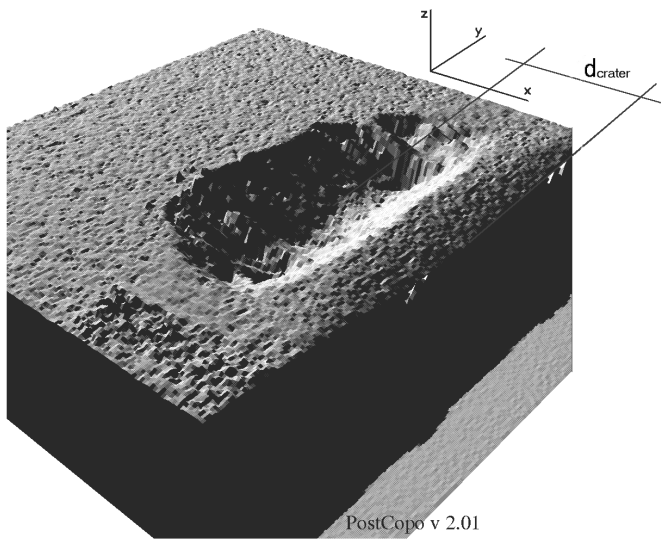


Figure 6. Lateral expansion in the orthogonal direction to the cutting plane



a) Numerical temperature contour plot on the tool flank face (only half of the tool is represented here)



b) Experimental three-dimensional mapping of the tool flank face

Figure 7. Temperature contour plot and wear effects

5.2. Oblique model

The second application concerns the numerical simulation of an oblique cutting process. In the presented model, we introduce an angle $\kappa = 75^\circ$, having in mind that κ is the angle between the edge of the tool and the cutting speed direction ($\kappa = 90^\circ$ in orthogonal cutting). The κ angle is best explained by referring to Figure 8. All the cutting parameters are the same as those used in the orthogonal model (see Table 1). Numerical results are reported in Table 5. In our model, δ is the average angle measured between the chip flow and the cutting plane. The introduction of 15° obliquity in the model ($\kappa = 75^\circ$) has an influence on all the results of the model. This causes the chip to flow in the direction $\delta = 48^\circ$. Proportionality between the κ and δ angles is quite linear and might be approximated by the relationship $\delta = 3 \left(\frac{\pi}{2} - \kappa \right)$. Temperatures are quite the same as those obtained with the orthogonal model. Cutting and advancing forces F_c and F_a have been reduced, but the lateral force F_z increases by a wide range.

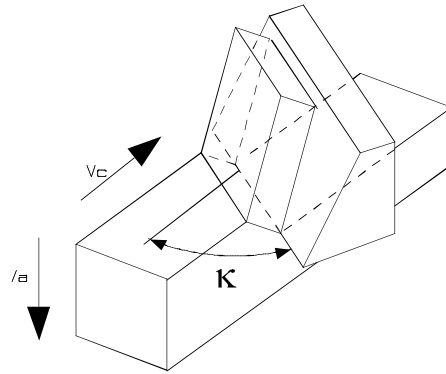


Figure 8. Representation of the oblique cutting process

F_c	1.811 kN	$T_{tool_{max}}$	700° C
F_a	0.381 kN	$T_{chip_{max}}$	900° C
F_z	0.539 kN	$L_{T_{max}}$	320 μm
L_{cont}	0.98 mm	δ	48°

Table 5. Numerical results of the oblique model

Figure 9 shows four representations of the chip at the end of the calculation. From this we can see the three-dimensional character of our model. Figure 10 represents Von-Mises' contour plot on the chip and the workpiece. Figure 11 shows the temperature contour plot on the rear face of the chip (the tool has been removed in this figure). The figure illustrates the helicoidal form of the chip induced by oblique cutting.

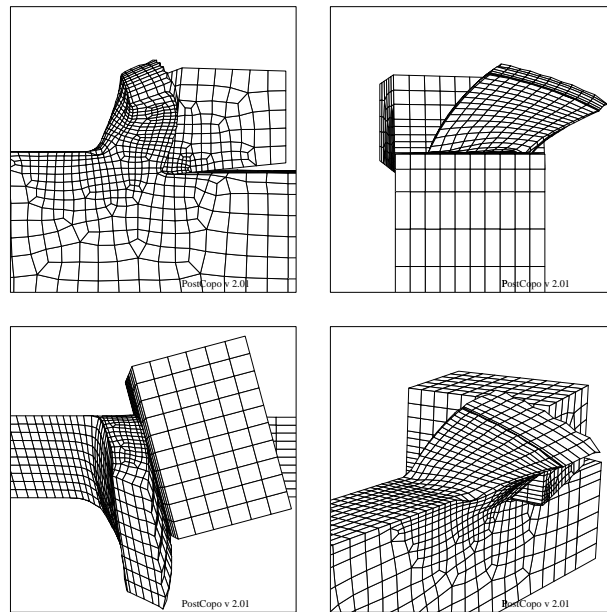


Figure 9. *Three-dimensional representations of the oblique cutting simulation results*

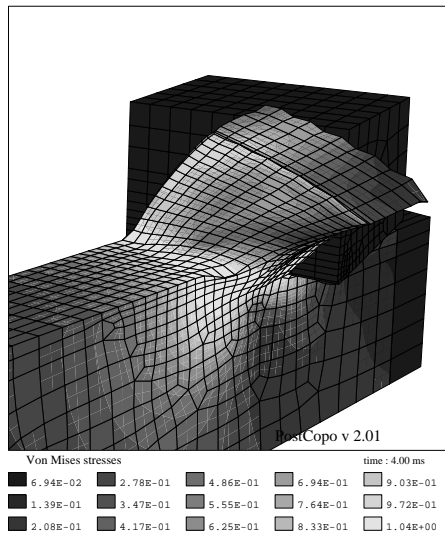


Figure 10. Von Mises contour plot of the oblique model with $\kappa = 75^\circ$

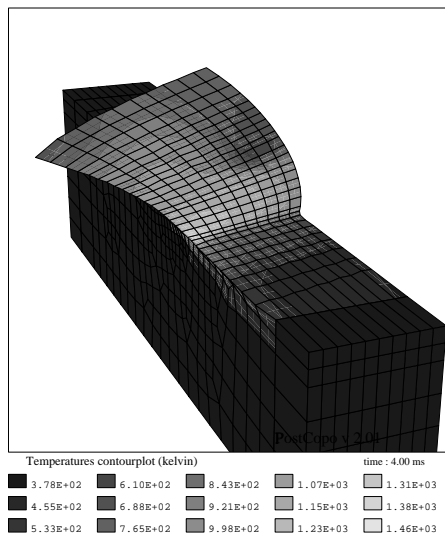


Figure 11. Temperature contour plot of the oblique model with $\kappa = 75^\circ$ (the tool has been removed in this figure)

6. Conclusion and perspectives

We developed a three-dimensional numerical model of an orthogonal and oblique metal cutting process based on an Arbitrary Lagrangian Eulerian approach. This provides a solution to remedy the problems linked to the classic Lagrangian and Eulerian formulations: severe meshing distortions in the Lagrangian description, unknown boundaries and contact conditions in the Eulerian approach. Different observations deduced from numerical results have been compared with available experimental results and give a good level of agreement. The originality of such a study is shown by the use of the ALE formulation and the development of a three-dimensional model. Comparison of this model with an analytical one shows the advantages of the numerical simulation based on less restrictive hypotheses. In addition, extensions of this work will include a better definition of the tool-chip contact law, including wear effects.

References

- BARDON J. P., Bases physiques des conditions de contact thermique imparfait entre milieux en glissement relatif¹. *Revue Générale de Thermique*, 33(386):83–91, 1994.
- [CHI 90] CHILDS T. H. C., MAEKAWA K., Computer-aided simulation and experimental studies of chip flow and tool wear in the turning of low alloy steels by cemented carbide tools. *Wear*, 139:235-250, 1990.
- [DON 82] DONEA J., GIULIANI S., HALLEUX J.P., An arbitrary Lagrangian-Eulerian finite element method for transient dynamic fluid-structure interactions. *Computer Methods in Applied Mechanics and Engineering*, 33:689–723, 1982.
- [HUE 90] HUETINK J., VREEDE P. T., Progress in mixed Eulerian-Lagrangian finite element simulation of forming processes. *International Journal for Numerical Methods in Engineering*, 30:1441-1457, 1990.
- [HUG 81] HUGHES T.J.R., LIU W.K., ZIMMERMANN K., Lagrangian-Eulerian finite element formulation for incompressible viscous flows. *Computer Methods in Applied Mechanics and Engineering*, 29:329–349, 1981.
- [JOH 83] JOHNSON R., COOK W.K., A constitutive model and data for metals subjected to large strains, high strain rates and high temperatures. *7th International Symposium on Ballistics, The Hague*, pages 541–547, 1983.
- [JOY 98] JOYOT P., RAKOTOMALALA R., PANTALE O., TOURATIER M., A numerical simulation of stationary metal cutting *Proc. Instn. Mech. Engrs. 212 part C* (pages 331-341, 1998).
- [KOM 91] KOMVOPOULOS K., ERPENBECK S.A., Finite element modelling of orthogonal metal cutting. *Journal of Engineering for Industry*, 112:253–267, 1991.
- [KOS 78] KOSLOFF D., FRAZIER G.A., Treatment of hourglass patterns in low order finite el-

¹ Physical bases of non perfect thermal sliding contact.

- ement codes. *International Journal for Numerical Methods in Engineering*, 2:57–72, 1978.
- [LEE 80] LEE E. H., Mc MEEKING R. M., Concerning elastic and plastic components of deformation. *International Journal of Solids and Structures*, 16:715–721, 1980.
- [LEZ 90] LEZANSKI P., SHAW M. C., Tool face temperatures in high speed milling. *Journal of Engineering for Industry*, 112:132-135, 1990
- [MAR 95] MARUSICH T.D., ORTIZ M., Modelling and simulation of high-speed machining. *International Journal for Numerical Methods in Engineering*, 38:3675–3694, 1995.
- [RAK 93] RAKOTOMALALA R., JOYOT P., TOURATIER M., Arbitrary Lagrangian-Eulerian thermomechanical finite element model of material cutting. *Communications in Numerical Methods in Engineering*, 9:975–987, 1993.
- [SHI 93] SHIH A.J. YANG H.T.Y. Experimental and finite element predictions of residual stresses due to orthogonal metal cutting. *International Journal for Numerical Methods in Engineering*, 36:1487–1507, 1993.
- [TAY 91] TAY A.A.O. The importance of allowing for the variation of thermal properties in the numerical computation of temperature distribution in machining. *Journal of Materials Processing Technology*, 28:49–58, 1991.
- [TAY 93] TAY A.A.O. A review of methods of calculating machining temperature. *Journal of Materials Processing Technology*, 36:225–257, 1993.
- [UED 93] UEDA K. MANABE K. Rigid-plastic FEM analysis of three-dimensional deformation field in chip formation process. *Annals of the CIRP*, 42-1:35-38, 1993.
- [YOU 92] YOUNIS M.A. Mechanical and thermal stresses in clamped, brazed, and bonded carbide tools. *Journal of Engineering for Industry*, 114:377–385, 1992.